Available online at www.sciencedirect.com
SCIENCE DIRECT
Journal of Magnetic Resonance 178 (2006) 297–307
JMR Journal of Magnetic Resonance
www.elsevier.com/locate/jmr

Sensitivity and resolution in proton solid-state NMR at intermediate deuteration levels: Quantitative linewidth characterization and applications to correlation spectroscopy

Donghua H. Zhou, Daniel T. Graesser, W. Trent Franks, Chad M. Rienstra *

Department of Chemistry, University of Illinois, 600 South Mathews Avenue, Urbana, IL 61801, USA

Received 4 September 2005; revised 14 October 2005
Available online 10 November 2005

Abstract

We present a systematic study of proton linewidths in rigid solids as a function of sample spinning frequency and proton density, with the latter controlled by the ratio of protonated and perdeuterated model compounds. We find that the linewidth correlates more closely with the overall proton density (ρ_H) than the size of local clusters of ^{1}H spins. At relatively high magic-angle spinning (MAS) rates, the linewidth depends linearly upon the inverse MAS rate. In the limit of infinite spinning rate and/or zero proton concentration, the linewidth extrapolates to a non-zero value, owing to contributions from scalar couplings, chemical shift dispersion, and B_0 field inhomogeneity. The slope of this line depends on the overall concentration of unexchangeable protons in the sample and the spinning rate. At up to 30% protonation levels ($\sim$2 ^{1}H/100 Å^3), proton detection experiments are demonstrated to have a substantial (2- to 3-fold) sensitivity gain over corresponding ^{13}C-detected experiments. Within this range, the absolute sensitivity increases with protonation level; the optimal compromise between sensitivity and resolution is in the range of 20–30% protonation. We illustrate the use of dilute protons for polarization transfer to and from low-γ spins within 5 Å, and to be utilized as both magnetization source and detection spins. The intermediate protonation regime enhances relaxation properties, which we expect will enable new types of ^{1}H correlation pulse sequences to be implemented with improved resolution and sensitivity.

Keywords: Indirect proton detection; Linewidth; Sensitivity; Signal-to-noise; Solid-state NMR

1. Introduction

Recent advances in biomolecular solid-state NMR (SSNMR) are highlighted by partial or full assignment of several small globular proteins (BPTI, ubiquitin, SH3 domain of α-spectrin, Crh, thioredoxin, mastoparan, GB1) [1–9] and the determination of complete high-resolution structures for peptides [10–12] and global folds of proteins (SH3 and kaliotoxin) [13,14]. Studies of membrane proteins at very low concentration (when reconstituted into liposomes) [15] or high molecular weight [1] illustrate the power of SSNMR to lend insight into previously inaccessible systems, but concurrently illustrate the fact that such experiments generally suffer from low sensitivity. This fact frustrates applications of sophisticated 3D experiments to many larger proteins and ultimately limits the impact of SSNMR on modern biology.

Sensitivity in solids is compromised primarily by the usual requirement of directly detecting low γ (gyromagnetic ratio) nuclei such as ^{13}C and ^{15}N. Indirect detection via ^{1}H is 8 and 30 times more sensitive than direct ^{13}C and ^{15}N detection, respectively, assuming the signal-to-noise ratio (SNR) is proportional to $\gamma^{3/2}$ [16]. Therefore, proton detection has become an indispensable component in most biological and organic solution NMR sequences [16]. The enhancement is inversely proportional to the square root of proton linewidth [17]; therefore the sensitivity gain is not always achievable in solid samples, because strong ^{1}H–^{1}H dipolar interactions broaden linewidths to the order

* Corresponding author. Fax: +1 217 244 3186.
E-mail address: rienstra@scs.uiuc.edu (C.M. Rienstra).

1090-7807/$ - see front matter © 2005 Elsevier Inc. All rights reserved.
doi:10.1016/j.jmr.2005.10.008

of 40 kHz. The reduction of ^{1}H linewidth is key to the success of proton detection in SSNMR.

Historically, line narrowing has been achieved by several different approaches. Windowed homonuclear decoupling for static solids [18] was the first approach, subsequently adapted for magic-angle spinning (MAS) experiments and dubbed CRAMPS (combined rotation and multiple-pulse spectroscopy) [19–22]. This approach yields high resolution but suffers from the requirement of large receiver bandwidths, which allow audio frequency noise to fold into the spectral region and compromise overall sensitivity. The relatively long pulse sequence cycle times of most CRAMPS sequences also interfere with spatial averaging by MAS. Pulsed spin-locking sequences enlarge the data sampling windows for static samples [23], increasing sensitivity by a factor of 1.8–2.5 for ^{15}N spectra. However, ^{1}H chemical shift resolution is sacrificed. This application is therefore best suited to samples for which resolution is not required in the directly detected ^{1}H dimension. In recent years, high speed (>20 kHz) MAS technology has become available, and enhancements of 1.5–2.5 versus ^{13}C detection and 2.0–3.2 versus ^{15}N detection have been demonstrated for fully protonated solids [17,24]. Unfortunately even at MAS rates >30 kHz, fully protonated samples still can have greater than 2 ppm homogeneous ^{1}H linewidths, so spinning alone is not sufficient to yield resolution competitive with solution NMR, even with the fastest spinners currently available [25–27]. Ultimately, the highest resolution and sensitivity have been demonstrated by combinations of isotopic spin dilution with high-speed MAS [28–32], yielding in optimal circumstances at 800 MHz a factor of ~7 in sensitivity enhancement versus ^{15}N detection and sub-ppm line widths in a highly ordered protein sample (ubiquitin) [32]. With this spin dilution approach, very high-resolution proton-detected ^{1}H–^{15}N correlation spectra have also been reported for two perdeuterated small proteins [30,32].

Clearly very fast MAS yields the highest sensitivity per unit sample, and is preferred in mass-limited scenarios; in this case, 2.5 mm or smaller diameter rotors are best utilized to maximize filling factor and MAS rate. However, the optimal experimental conditions are less clear in cases where sufficient quantities of protein can be prepared to fill larger diameter (3.2–5.0 mm) rotors (volumes of ~20 to >100 μL). Likewise, very low (~1–3%) levels of proton enrichment yield the best resolution [33–35], but since the linewidths in that regime are dominated by other (principally inhomogeneous) factors, acceptable tradeoffs in resolution might be possible with slightly higher ^{1}H concentrations (~10–30%); the larger number of total protons might also increase absolute sensitivity. The current study aims to shed light on these fundamental issues, in order to optimize *absolute* sensitivity for biological macromolecules.

On a practical level, most ^{1}H spin dilution schemes for proteins so far have been implemented under the assumption that a high level of ^{2}H could be incorporated into the bacterial growth media, and ^{1}H exchange achieved during purification and/or refolding. However, in tightly folded proteins and/or membrane proteins, this approach suffers from the complication that rates of proton exchange can vary by orders of magnitude, and up to 80% of total amide sites, corresponding to those buried in the membrane, have been reported to be protected from $^{1}H/^{2}H$ exchange [36–42]. Therefore, it is not always possible to control the level of protonation precisely on a site-by-site basis. Understanding the resulting variations in linewidths and signal intensities will be helpful for interpreting ^{1}H spectra in such systems.

To lend insight into this problem, and explore the general problem of ^{1}H spectroscopy in the intermediate protonation and MAS regimes, we have acquired and analyzed spectra of several model compounds in which the level of protonation could be well controlled. The use of relatively simple model compounds permits precise measurements of line widths and sensitivity to be made over a large range of spinning rates, including several conditions where protein signals are poorly resolved. The extracted linewidths and peak heights as a function of spinning rate depend upon protonation level in a systematic way that will aid future sample and pulse sequence design in partially deuterated solid proteins.

2. Results and discussion

In Fig. 1 for a D_2O-recrystallized sample of 10:90 $CD_3CHND_3^+COO^-/CD_3CDND_3^+COO^-$, ^{1}H spectra of direct ^{1}H polarization (DP) and reverse cross-polarization (RCP) [43] from ^{2}H to ^{1}H are compared. The DP spectrum

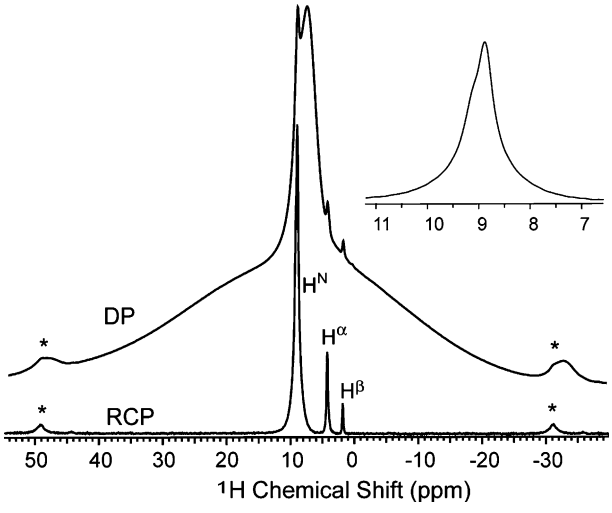

Fig. 1. 500 MHz ^{1}H spectra of a D_2O-recrystallized 10:90 mixture of $CD_3CHND_3^+COO^-/CD_3CDND_3^+COO^-$ at 20 kHz MAS frequency. On top is the one pulse ^{1}H Bloch decay (or direct polarization, DP) spectrum (32 scans). The bottom spectrum is acquired with reverse cross-polarization (RCP) from ^{2}H to ^{1}H (512 scans) [43]. The RCP spectrum is free of background signals seen in the DP spectrum. Spectra were processed without apodization. The inset is expansion around the amine peak in the RCP spectrum. Asterisks mark spinning side bands.

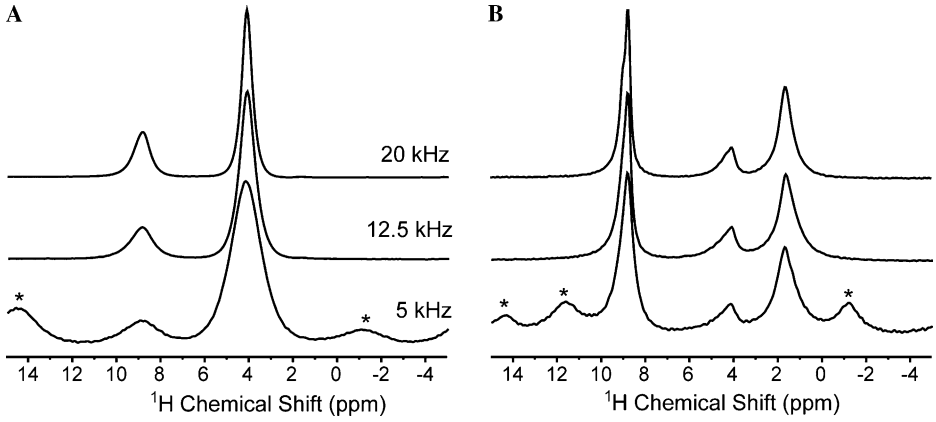

Fig. 2. 500 MHz ^{1}H spectra at several MAS frequencies of (A) $CD_3CHND_3^+COO^-$ and (B) a mixture of 20:80 $^{13}CH_3{}^{13}CH^{15}ND_3^+COO^-$/$CD_3CDND_3^+COO^-$, recrystallized from D_2O solution. Each spectrum was acquired with 1024 transients and processed without apodization. Asterisks mark spinning side bands.

suffers from a very strong probe background signal (in this quadruple resonance probe, designed for ^{1}H–^{13}C–^{2}H–^{15}N operation with ^{13}C or ^{15}N detection, the ^{1}H background has not been minimized). The spectrum contains a relatively narrow component from around 2 to 12 ppm and a very broad component from −30 to 45 ppm. Peaks from samples of small quantity or low proton content are barely apparent above the background signal. RCP essentially removes such background signal since the rotor parts are not deuterated. Therefore, only RCP 1D ^{1}H spectra are used in the following linewidth characterization. (The β-proton peak comes from residual protons in $CD_3CDND_3^+COO^-$, not from $CD_3CHND_3^+COO^-$ since this peak is absent for the 100% $CD_3CHND_3^+COO^-$ sample in Fig. 2A.)

Fig. 2 shows ^{1}H MAS spectra as a function of MAS rate for two samples: $CD_3CH(ND_3^+)COO^-$ ("$^{1}H_1$-Ala") and a 20:80 mixture of $^{13}CH_3{}^{13}CH(^{15}ND_3^+)^{13}COO^-$ ("^{13}C,^{15}N,$^{1}H_4$-Ala") and $CD_3CD(ND_3^+)COO^-$ ("U-^{2}H-Ala"). In Fig. 2A, spectra of the 100% $^{1}H_1$-Ala sample show the residual amine proton peak (around 9 ppm) besides the α-proton peak (~4 ppm). The peaks progressively become broader as the spinning rate decreases; the full width at half maximum (FWHM) of the amine peak is 420, 585, and 1085 Hz, and of H^{α} is 270, 410, and 825 Hz at spinning rates 20, 12.5, and 5 kHz, respectively. These 1D ^{1}H spectra follow the well-understood trend of narrowing in proportion to the MAS rate [44–47]. In Fig. 2B, the 20% ^{13}C,^{15}N,$^{1}H_4$-Ala sample has three peaks (H^{N}, H^{α}, and H^{β}). The linewidths at the three spinning rates are 217, 237, and 368 Hz for the amine protons, 379, 512, and 940 Hz for H^{α}, and 352, 447, and 583 Hz for H^{β}.

The amine peak in Fig. 2B for the 20% ^{13}C,^{15}N,$^{1}H_4$-Ala sample clearly manifests an asymmetric lineshape as has been observed by McDermott et al. [28] for a 99% deuterated alanine sample. It was attributed to incompletely averaged dipolar coupling to the quadrupole ^{14}N nuclei, similar to the well known ^{13}C–^{14}N asymmetric doublet [48]. The same peak asymmetry is observed for all other samples, including 10% $^{1}H_1$-Ala in Fig. 1 inset, except for the 100% $^{1}H_1$-Ala sample (Fig. 2A). We attribute the symmetry for the latter sample to the strong dipolar coupling with α-proton, which has maximal density in this sample. In each 100 Å^3 volume, the 10% and 100% $^{1}H_1$-Ala samples have an average of 0.79 and 0.39 amine protons, and 0.09 and 0.92 α-protons, respectively (see Table 1 below). Therefore, for a molecule in the 10% sample, most amine protons ($^{1}H^{N}$) have an α-deuteron ($^{2}H^{\alpha}$) while in the 100% sample every amine proton has an α-proton. If the residual dipolar coupling to α-proton is stronger than that to ^{14}N, we would expect the greatest line width in the 100% $^{1}H^{\alpha}$-Ala sample, as observed in the experiments.

In Fig. 3, the H^{α} and H^{β} center band linewidths as a function of rotor period are shown for alanine of various

Table 1
Slope k and intercept b parameters from Fig. 3, with standard errors in parentheses

Sample	Proton density (^{1}H/100 Å^3)			H^{α}		H^{β}	
	Nominal	$\rho(H^{C})$	$\rho(H^{N})$	k (Hz/ms)	b (Hz)	k (Hz /ms)	b (Hz)
30% ^{13}C,^{15}N,$^{1}H_4$-Ala	1.12	1.12	0.87	6728 (1000)	189 (64)	5177 (346)	188 (22)
100% $^{1}H_1$-Ala	0.92	0.92	0.39	4302 (92)	62 (8)	NA	NA
20% ^{13}C,^{15}N,$^{1}H_4$-Ala	0.74	0.74	0.66	4097 (695)	181 (45)	3083 (280)	188 (22)
10% ^{13}C,^{15}N,$^{1}H_4$-Ala	0.38	0.38	0.75	1155 (118)	170 (10)	1323 (205)	190 (18)
5% ^{13}C,^{15}N,$^{1}H_4$-Ala	0.18	0.18	1.36	1331 (261)	158 (19)	816 (336)	201 (25)
10% $^{1}H_1$-Ala	0.09	0.13	0.79	1053 (37)	80 (3)	777 (58)	59 (5)
5% $^{1}H_1$-Ala	0.05	0.06	0.69	970 (57)	66 (5)	673 (39)	60 (3)

Nominal, carbon-attached [$\rho(H^{C})$], and nitrogen-attached [$\rho(H^{N})$] proton densities are defined in the text.

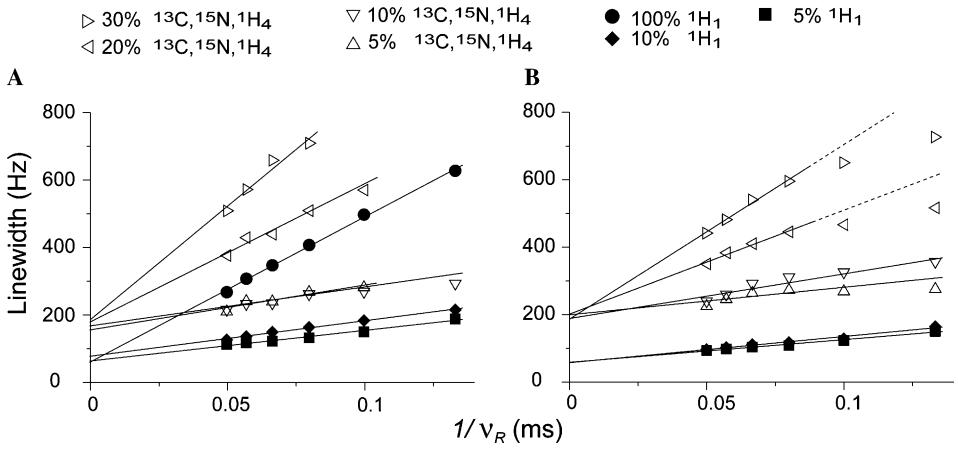

Fig. 3. Alanine (A) H^{α} and (B) H^{β} linewidths as a function of inverse spinning rate for samples of various proton densities. Spinning frequencies range from 7.5 to 20 kHz in step of 2.5 kHz. Linear fit parameters are summarized in Table 1. Data points under the dotted lines were not used in the fits.

proton densities. The linewidths are extracted by simultaneously fitting all peaks in a spectrum by Lorentzian components, whose width, position, and amplitude are subject to optimization, using spectrum modeling software DMFIT [49]. For both H^{α} and H^{β}, the linewidth is linear with the inverse spinning rate above 7.5 kHz; the 5 kHz data tend to be inaccurate due to low resolution and are therefore excluded from further analysis. Previously it has been reported for a small peptide, adamantane and polycarbonate that in the fast spinning regime the residual dipolar linewidth is inversely proportional to the spinning rate [29,44,45]. We observe a similar trend; however, the *y*-intercepts of the fitted lines in Fig. 3 do not vanish, implying that even infinite MAS rate cannot remove all line broadening. We attribute this line broadening to inhomogeneous factors, including static field inhomogeneity (~16 Hz at the ^{1}H frequency, based on 4 Hz ^{13}C linewidth in the adamantane standard used for shimming this probe) sample heterogeneity (chemical shift dispersion) and scalar couplings to ^{2}H, ^{15}N, and ^{13}C. The intercepts are very different for the two sample series: ~60 Hz for $^{1}H_1$-Ala samples and ~190 Hz for $^{13}C,^{15}N,^{1}H_4$-Ala samples; their difference is close to the expected one bond ^{1}H–^{13}C coupling (~135 Hz). As in the 2D experiments shown below, the ^{1}H–^{13}C scalar coupling can be decoupled by rotor synchronized π pulses on the ^{13}C channel.

The slope *k* and intercept *b* parameters for the linear fits are listed in Table 1, in the order of decreasing nominal proton density (ρ_H, expressed as the number of protons per 100 Å^3). The nominal proton density is calculated assuming each constituent of the mixture was 100% pure and all amine protons are exchanged with deuterons, and using $\rho_H = 6.5\ ^{1}H/100\ Å^3$ for fully protonated Ala according to crystal structure [50]. The nitrogen-attached proton density $\rho(H^N)$ is calculated by multiplying the nominal density by a correction factor, which is the ratio of integrated intensities for the amine peak and the anticipated peaks under the ideal conditions assumed above (H^{α} peak for $^{1}H_1$-Ala, H^{α} and H^{β} peaks for $^{13}C,^{15}N,^{1}H_4$-Ala). The 10 and 5% $^{1}H_1$-Ala samples have a small H^{β} peak, resulting from an isotopic impurity in $CD_3CDND_3^{+}COO^{-}$; they are taken into account to when calculating carbon-attached proton density $\rho(H^C)$.

The slope parameters *k* in Table 1 are plotted as a function of carbon-attached and total proton densities (sum of $\rho(H^C)$ and $\rho(H^N)$) in Figs. 4A and B, respectively. The parameter *k* correlates very well with $\rho(H^C)$ as shown in Fig. 4A. For example, the slope $k(H^{\alpha})$ for the 100% $^{1}H_1$-

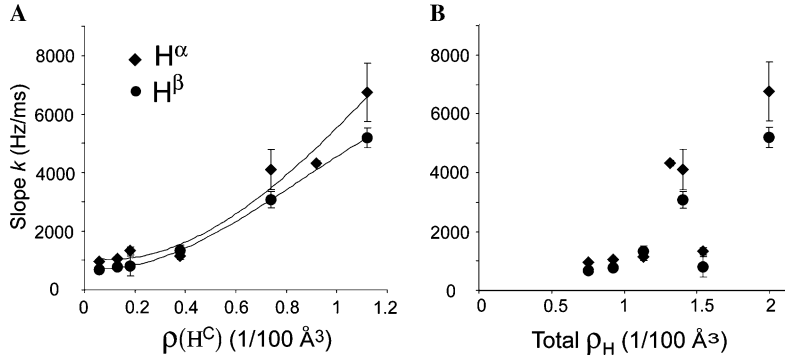

Fig. 4. The slope parameter *k* in Table 1 plotted as a function of (A) carbon-attached proton density $\rho(H^C)$ and (B) total proton density. Fit parameters were extracted from experiments shown in Fig. 3.

Ala sample ($\rho(H^C) = 0.92$) falls in between the values of 1.12 and 0.74 observed for 30 and 20% $^{13}C,^{15}N,^{1}H_4$-Ala, respectively. This trend follows the order of proton density, even though the linewidth of the 100% $^{1}H_1$-Ala is less than those of the two $^{13}C,^{15}N,^{1}H_4$-Ala samples. The correlation to total proton density (Fig. 4B) or amine proton density alone (not shown) is poorer.

Fig. 4 also illustrates that the slope k depends more on the overall average carbon-attached than local proton density; for example, the 10% $^{13}C,^{15}N,^{1}H_4$-Ala (0.38 ^{1}H/100 Å^3 carbon-attached proton density) has $k = 1155$ Hz/ms, despite nearby methyl protons, whereas the 100% $^{1}H_1$-Ala sample has (with no strong couplings yet a 0.92 ^{1}H/100 Å^3 density) $k = 4302$ Hz/ms.

2.1. 2D experiments

The narrow proton linewidth of the diluted samples makes indirect detection advantageous. First, this is demonstrated by the ^{1}H-detected HETCOR spectra of a fully protonated Ala sample and the 10% $^{13}C,^{15}N,^{1}H_4$-Ala sample in Figs. 5A and B, respectively. Though the diluted sample has only around 10% proton content of the fully protonated sample, it has up to 3.5-fold enhancement in sensitivity and resolution. These comparisons are for the same number of scans and pulse delay. The longitudinal relaxation time T_1's (ranging from 0.3 to 0.5 s for samples of 10% and higher proton content) of the magnetically diluted samples is only marginally greater than the natural abundance samples; similar results were observed recently in extensively deuterated ubiquitin [51]. Furthermore, this is demonstrated by the comparison of the ^{1}H- and ^{13}C-detected HETCOR spectra in Figs. 5B and C, respectively. The ^{1}H detection significantly improves sensitivity for nearly all peaks, including C^{α}–H^{α} (1975 for ^{1}H-detection vs. 906 for ^{13}C-detection, 2.2-fold enhancement) and C^{β}–H^{β} (5789 vs. 2349, 2.5-fold). The SNR of the peak at (9, 23) ppm for the correlation of the amine $^{1}H^{N}$ and methyl $^{13}C^{\beta}$ increases

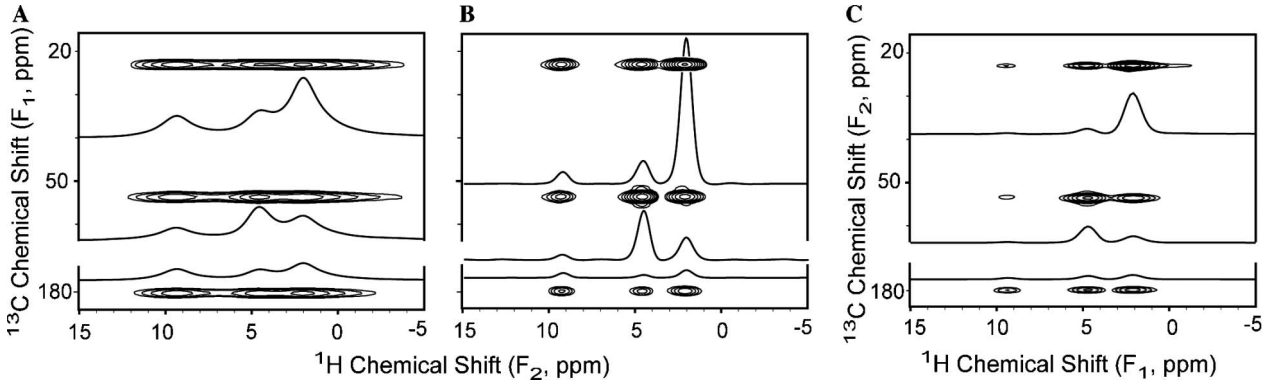

Fig. 5. HETCOR spectra of alanine samples. ^{1}H-detected spectra of 10% $^{13}C,^{15}N,^{1}H_4$-Ala mixed with (A) protonated alanine, (B) 10% $^{13}C,^{15}N,^{1}H_4$-Ala recrystallized with deuterated alanine, and (C) ^{13}C-detected spectrum of the second sample. Spinning frequency was 22.727 kHz, 4 scans were acquired for each row, and a recycle delay was 1 s. The ^{1}H-detected experiments have 22 μs × 512 pts in t_1 (^{13}C, TPPI) 22 μs × 2048 pts in t_2 (^{1}H). The ^{13}C–^{1}H scalar coupling was removed via a rotor-synchronized ^{13}C π pulse decoupling scheme. The ^{13}C-detected experiment has 11 μs × 512 pts in t_1 (^{1}H, TPPI) 11 μs × 4096 pts in t_2 (^{13}C). Spectra were processed with 0.5 ppm Lorentzian-to-Gaussian apodization in each dimension (−0.2 ppm Lorentzian plus 0.7 ppm Gaussian line broadening). Contours were drawn starting from 20 times the root mean square noise level, and separated by a factor of two. The slices are drawn at identical scales.

Table 2
Signal-to-noise ratio for proton- (SNH) and carbon-detected (SNC) HETCOR spectra and enhancement factor (ξ = SNH/SNC) for five alanine samples

	H^N					H^{α}					H^{β}				
	a	b	c	d	e	a	b	c	d	e	a	b	c	d	e
C^{β}															
SNH	342	482	971	1951	553	359	930	1928	2610	676	2330	5789	10191	13270	1621
SNC	75	51	126	277	277	125	324	721	1137	362	1012	2349	4331	5935	934
ξ	4.6	9.5	7.7	7.0	2.0	2.9	2.9	2.7	2.3	1.9	2.3	2.5	2.4	2.2	1.7
C^{α}															
SNH	191	226	485	882	305	791	1975	4246	5795	870	358	899	1916	2687	632
SNC	53	39	85	173	146	364	906	1965	2792	518	153	378	741	1012	243
ξ	3.6	5.8	5.7	5.1	2.1	2.2	2.2	2.2	2.1	1.7	2.3	2.4	2.6	2.7	2.6
CO															
SNH	146	189	377	763	284	47	115	242	358	276	119	303	618	974	445
SNC	104	95	224	520	250	82	220	511	808	243	109	278	563	881	251
ξ	1.4	2.0	1.7	1.5	1.1	0.6	0.5	0.5	0.4	1.1	1.1	1.1	1.1	1.1	1.8

Samples a to d are 5, 10, 20, and 30% $^{13}C,^{15}N,^{1}H_4$- Ala in U-^{2}H-Ala, sample e is 10% $^{13}C,^{15}N,^{1}H_4$-Ala in protonated Ala. All spectra are processed with matched line broadening of 0.5 ppm in each dimension.

by 9.5 times (482 vs. 51). We attribute a factor of ~2.5 to the gain of ^{1}H- vs. ^{13}C-detection sensitivity (as seen for other peaks). Another factor of ~4 comes from the more favorable starting polarization in the ^{1}H-detected experiment, in which all protons transfer polarization to the methyl ^{13}C, while in the ^{13}C-detected experiment only polarization from amine protons is transferred. The 5.8-fold (226 vs. 39) increase for the amine $^{1}H^{N}$ and the $^{13}C^{\alpha}$ correlation peak at (9 ppm, 53 ppm) can be explained similarly.

The SNR's for all nine peaks are listed in Table 2 for five samples of various proton density. The absolute SNR's (both SNH for proton detection and SNC for carbon detection) are largest for the four heteronuclear correlation peaks among H^{α}, H^{β} and C^{α}, C^{β}, which are one or two bonds apart. These peaks also have large enhancement factor ξ from 2.1 to 2.9 for all the four proton diluted samples (5, 10, 20, and 30% ^{13}C,^{15}N,$^{1}H_4$-Ala). Nevertheless, these values are much smaller than the predicted factor of 8, which has been achieved by solution NMR. Two factors may contribute to this less than ideal result: (1) the proton linewidth remains broader than in solution state, (2) only about 40% of the polarization transfers back from ^{13}C to ^{1}H, due to B_1 inhomogeneity among other factors [24,32,52].

For the four proton diluted samples, the absolute SNR continued increasing linearly with the percentage of the ^{13}C and ^{1}H labeling up to approximately 1 ^{1}H /100 Å$_3$. The SNR decreases with higher proton densities; for example, the 10% ^{13}C,$^{1}H_4$-Ala in fully protonated Ala sample has much lower SNR than the 10% ^{13}C,^{15}N,$^{1}H_4$-Ala in deuterated Ala, only 28% SNR in the worst case for the H^{β}–C^{β} peak. Even for the fully protonated sample, ξ ranges from 1.7 to 2.6, in agreement with the 1.5–2.5 enhancements observed in the high speed MAS study by Ishii et al. [17,24]. Our results show that an additional factor of 4 can be achieved (per ^{13}C,^{15}N-labeled spin) by diluting the sample in ^{2}H-labeled material. In this context, the *absolute* sensitivity of the ^{1}H-detected HETCOR experiment on the ^{1}H,^{13}C,^{15}N-labeled molecule will be higher than if the entire sample volume had contained ^{1}H,^{13}C,^{15}N material. Furthermore, the resolution will be substantially better. The average proton linewidths in ^{13}C–^{1}H spectra are 200, 260, 310, and 1100 Hz for the 10, 20, 30, and 100% (here the 10% ^{13}C,^{15}N-labeled Ala in proton background) protonated samples, respectively. To consider both sensitivity and resolution, we define a merit score to be SNH divided by proton line width. The scores are 29, 39, 42, 15 for the C^{β}–H^{β} peak and 10, 16, 19, and 8 for the C^{α}–H^{α} peak, in the order of increasing proton levels 10, 20, 30, and 100% (the scores for the 100% sample has been multiplied by a factor of 10 to extrapolate to 100% ^{13}C labeling). The best merit score is found at approximately 50% ^{13}C,^{1}H; at 30% protonation there is only a marginal sacrifice in sensitivity, but with improved resolution. Erring on the side of lower protonation will be favorable for samples containing fewer methyl groups.

Examining the ^{13}C sites that are not directly bonded to protons reveals smaller enhancements. All peaks correlating to CO have very low SNR and ξ, especially $\xi < 1$ for the H^{α} to CO correlation. This is due to inefficient CO to ^{1}H cross-polarization transfer. H^{N} to ^{13}C correlation peaks also have rather low absolute SNR, due to lower CP efficiency from the rotating amine group. For instance, both H^{N} and H^{β} are two bonds away from C^{α}, but SNR of H^{N} to C^{α} peak is approximately five times weaker than the H^{β} to C^{α} peak.

2.2. N-Acetyl-valine

To examine the properties described above on a larger molecule, a series of samples was prepared by diluting uniformly ^{13}C,^{15}N-labeled *N*-acetyl valine (^{13}C,^{15}N-NAV) in deuterated NAV (U-^{2}H-NAV); this system has substantial local clusters of 13 protons. Fig. 6 shows ^{1}H MAS spectra at 22.7 kHz for NAV samples with various proton densities. The β-proton (3.3 ppm) and the acetyl methyl peaks (2.7 ppm) are close to each other, and indistinguishable at even relatively small (5%) protonation levels. In contrast, the two γ peaks (1.8 and 1.3 ppm) can be resolved even at 20% protonation.

HETCOR spectra for NAV samples are shown in Fig. 7. Proton detection significantly increases the SNR as demonstrated by ^{13}C–^{1}H HETCOR (Fig. 7A) and ^{1}H–^{13}C

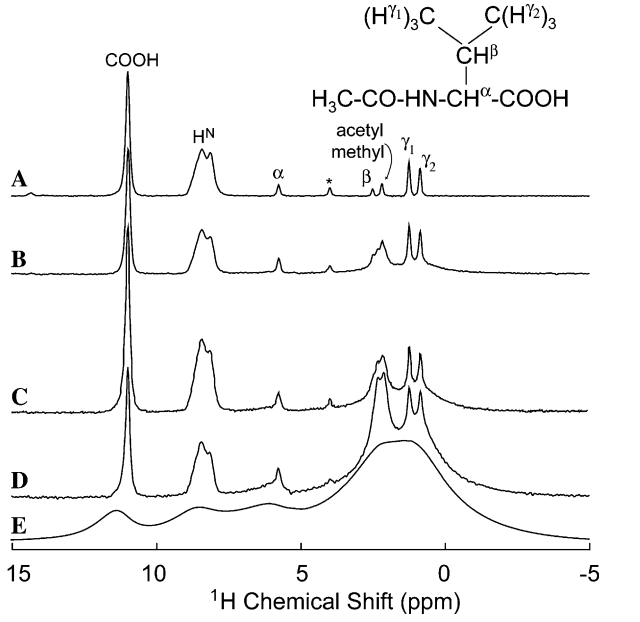

Fig. 6. ^{1}H MAS spectra at 22.7 kHz of various *N*-acetyl-valine (NAV) samples: (A) residual protons (<1%) in uniformly deuterated NAV (U-^{2}H-NAV) (B) 5% ^{13}C,^{15}N-NAV in U-^{2}H-NAV, (C) 10% ^{13}C,^{15}N-NAV in U-^{2}H-NAV, (D) 20% ^{13}C,^{15}N NAV in U-^{2}H-NAV, and (E) 20% ^{13}C,^{15}N-NAV in fully protonated NAV. (A–D) Acquired with ^{2}H to ^{1}H reverse CP, 1024 scans, 0.25 s recycle delay. (E) Single pulse proton Bloch decay, 8 scans. The asterisk marks a residual water peak.

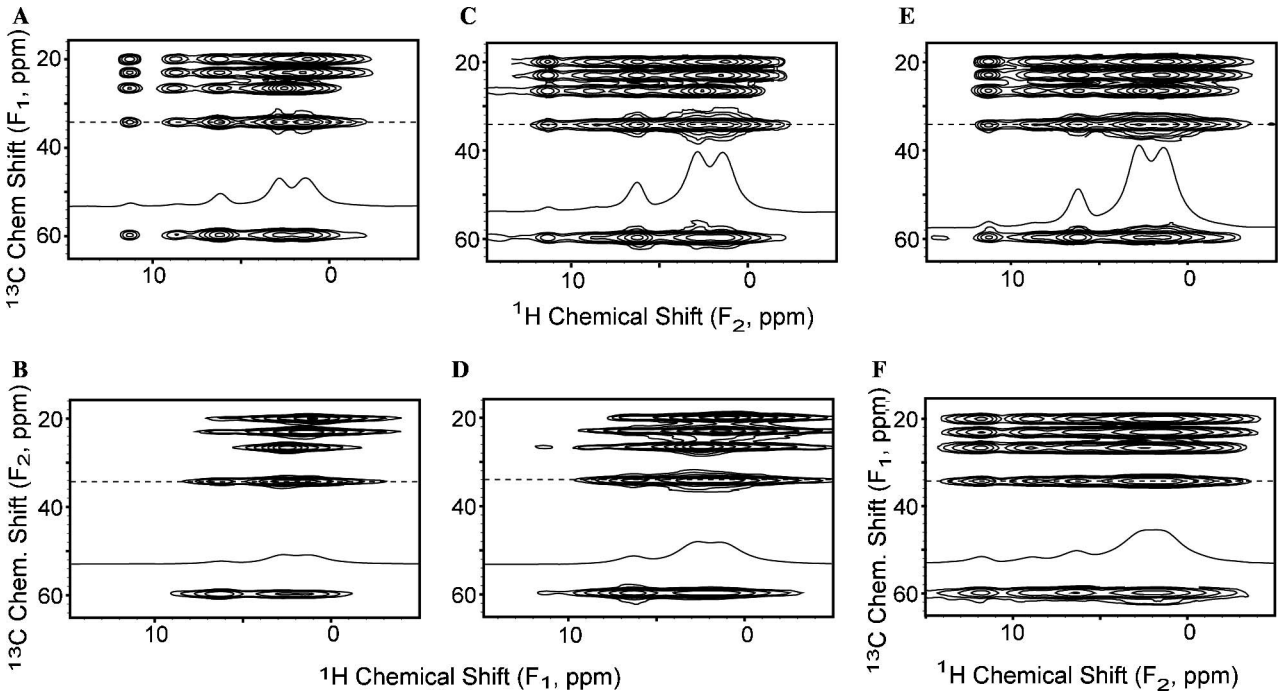

Fig. 7. HETCOR spectra of NAV samples. ^{1}H-detected spectra of (A) 10% ^{13}C,^{15}N-NAV in deuterated background, (C) 20% ^{13}C,^{15}N-NAV in deuterated background, (E) 30% ^{13}C,^{15}N-NAV in deuterated background, and (F) 20% ^{13}C,^{15}N-NAV in protonated background; ^{13}C-detected spectra of the first sample (B) and second sample (D). In all cases, the stated percentage of ^{1}H,^{13}C,^{15}N-NAV was diluted in perdeuterated (or protonated) NAV, and the mixture recrystallized from deuterated (or protonated) methanol, as described in Section 3. Spinning frequency was 22.727 kHz, with 4 scans per row, and a recycle delay of 1 s. Spectra were acquired and processed with the same parameters as in Fig. 5. Contours were drawn starting from 10 times the root mean square noise level, and separated by a factor of two. The slices are drawn at identical scale.

(Fig. 7B) spectra for the sample of 10% ^{13}C,^{15}N-NAV in deuterated background, and Figs. 7C and D for the sample of 20% ^{13}C,^{15}N-NAV in deuterated background. The signal intensity increases with content of ^{13}C and ^{1}H, as demonstrated by the ^{13}C–^{1}H HETCOR spectra in Figs. 7A, C, E for 10, 20, and 30% ^{13}C and ^{1}H labeling, respectively. Fig. 7F is a ^{13}C–^{1}H HETCOR spectrum for the sample of 20% ^{13}C,^{15}N-NAV in proton background. The high density of protons results in very broad linewidths and low sensitivity as compared to Fig. 7C for the 20% ^{13}C,^{15}N-NAV in deuterated background.

SNR for 25 selected peaks are listed in Table 3 for four samples: the 10, 20, and 30% ^{13}C,^{15}N-NAV in deuterated background, and 20% ^{13}C,^{15}N-NAV in protonated background. For the three proton diluted samples, the proton-detection enhances SNR by $\xi = 2.0$–3.1 for most peaks. The peaks correlating CO or HN have weak SNR. In general, the same trends follow as for the Ala samples discussed in detail above, and despite the relatively large size of this proton cluster, the overall sensitivity and resolution enhancements observed in the intermediate protonation regime are substantial. Furthermore, the methyl protons are well correlated to all ^{13}C nuclei in the NAV molecule, even though the longest distance is 5 Å between γ-protons and the carbonyl carbon. This proves the feasibility of using methyl protons as polarization source and detection target in methyl-specific protonated protein samples.

3. Experimental section

Alanine samples were prepared with defined proton density by diluting $^{13}CH_3{}^{13}CH(^{15}ND_3{}^{+})^{13}COO^{-}$ (^{13}C,^{15}N,$^{1}H_4$-Ala) or $CD_3CH(ND_3{}^{+})COO^{-}$ ($^{1}H_1$-Ala) into $CD_3CD(ND_3{}^{+})COO^{-}$ (U-^{2}H-Ala). Exchangeable ^{1}H sites were exchanged to ^{2}H by several recrystallizations from $^{2}H_2O$ in a desiccator continuously purged with nitrogen gas. Crystals were crushed and packed into NMR rotor at atmospheric conditions. *N*-Acetyl valine (NAV) was synthesized via solution methods and recrystallized in deuterated methanol and $^{2}H_2O$. All amino acids were L-chiral, 98% isotopically labeled (except for the 99% 3,3,3-D3 Ala) and purchased from Cambridge Isotope Laboratories (Andover, MA). Samples were packed in 3.2 mm NMR rotors (Varian NMR, Palo Alto, California).

Experiments were carried out at a nominal temperature of 10 °C on a 500 MHz Infinity Plus spectrometer (Varian NMR) equipped with a ^{1}H–^{13}C–^{2}H–^{15}N probe. This probe is optimized for ^{13}C detection with $B_1^{H}/B_1^{C} = 0.26$, where B_1^{H} and B_1^{C} are the radio frequency magnitude normalized for unit input power for ^{1}H and ^{13}C channels, respectively [32]. Proton π/2 pulse widths were typically 3 μs in the Bloch decay experiments. In the RCP experiments, the ^{2}H π/2 pulse width was 5 μs; reverse cross-polarization was achieved by setting the ^{2}H field to ~46 kHz and optimizing the ^{1}H power level for each spinning frequency. The HETCOR 2D experiments employed pulse sequences sim-

Table 3
Signal-to-noise ratio for proton- (SNH) and carbon-detected (SNC) HETCOR spectra and enhancement factor ($\xi = \mathrm{SNH/SNC}$) for four *N*-acetyl-valine (NAV) samples

	H^N				H^α				H^β				$H_{\text{acetyl methyl}}$				$H^{\gamma 1}$			
	a	b	c	d	a	b	c	d	a	b	c	d	a	b	c	d	a	b	c	d
$C^{\gamma 1}$																				
SNH	58	125	155	128	201	477	615	217	550	1332	1759	587	333	1577	2174	739	1372	2628	3474	1056
SNC	NA	12	23	84	34	93	138	125	216	489	611	418	280	628	776	484	621	1300	1610	624
ξ	NA	10	6.7	1.5	5.9	5.1	4.5	1.7	2.5	2.7	2.9	1.4	1.2	2.5	2.8	1.5	2.2	2.0	2.2	1.7
$C_{\text{acetyl met}}$																				
SNH	60	118	139	161	87	310	418	214	Not resolved with $H_{\text{acetyl methyl}}$				2995	5235	6343	1079	333	928	1833	1057
SNC	9	14	33	121	8	27	52	99					972	2029	2396	594	185	552	861	447
ξ	6.7	8.4	4.2	1.3	11	11	8.0	2.2					3.1	2.6	2.6	1.8	1.8	1.7	2.1	2.4
C^β																				
SNH	35	84	93	98	209	504	710	189	465	1036	1478	411	Not resolved with H^β				469	1025	1466	562
SNC	9	24	34	73	64	154	225	126	210	463	595	258					205	461	596	265
ξ	3.9	3.5	2.7	1.3	3.3	3.3	3.2	1.5	2.2	2.2	2.5	1.6					2.3	2.2	2.5	2.1
C^α																				
SNH	41	88	103	101	400	864	1211	277	217	559	851	275	Not resolved with H^β				229	577	871	356
SNC	16	40	63	104	158	381	519	224	90	206	277	155					89	204	277	151
ξ	2.6	2.2	1.6	1.0	2.5	2.3	2.3	1.2	2.4	2.7	3.1	1.8					2.6	2.8	3.1	2.4
CO																				
SNH	72	87	132	201	54	127	196	178	276	610	869	467	383	739	1049	587	179	439	793	756
SNC	29	42	67	218	60	167	228	157	211	482	582	331	274	608	733	355	140	360	500	351
ξ	2.5	2.5	2.1	2.0	0.9	0.9	0.8	0.9	1.1	1.3	1.3	1.5	1.4	1.4	1.2	1.4	1.7	1.3	1.2	1.6

Samples a to c are 10, 20, 30% ^{13}C,^{15}N-NAV in U-^{2}H-NAV, sample d is 20% ^{13}C,^{15}N-NAV in protonated NAV. All spectra are processed with 0.5 ppm line broadening in each dimension.

ilar to those of Ishii at 22.7 kHz spinning frequency [17] with 75 kHz TPPM decoupling during ^{13}C evolution [53]. To remove ^{13}C–^{1}H scalar couplings in the proton-detected HETCOR, a train of rotor-synchronized ^{13}C π pulses (width 8 μs) was applied during acquisition; in the ^{13}C-detected HETCOR, a single ^{13}C π pulse was applied in the middle of ^{1}H evolution period. For cross-polarization, ^{1}H was at 75 kHz and ^{13}C tangent-ramped from 50 to 75 kHz; a 1 ms contact time was used for the ^{1}H to ^{13}C polarization transfer, and in the proton detection experiment 3 ms was used for the ^{13}C to ^{1}H transfer to maximize overall intensity. In the ^{13}C–^{1}H experiments, 512 points in t_1 (^{13}C, TPPI) and 2048 points in t_2 (^{1}H) were acquired with 22 μs dwell time in both dimensions. In the ^{1}H–^{13}C experiments, 512 points in t_1 (^{1}H, TPPI) and 4096 pts in t_2 (^{13}C) were acquired with dwell time of 11 μs in both dimensions.

4. Conclusions

In this study, samples with defined proton densities were prepared by diluting protonated Ala or NAV into a perdeuterated background, enabling examination of resolution and sensitivity in solid-state proton detection in clusters consisting of 4 or 13 protons. The proton linewidth is linear with rotor period at spinning rates above 10 kHz. The slope of this line increases with overall proton density; the size of local cluster has a lesser effect. The non-zero intercept is attributed to scalar couplings, B_0 field inhomogeneity, and sample heterogeneity. As a caveat, the Ala and NAV samples studied here have relatively high content of methyl protons. The rapid rotation of CH_3 renders the ^{1}H–^{1}H dipolar interaction within the methyl group inhomogeneous. Systems with more CH and CH_2 content might have broader linewidths and a stronger dependence on the local cluster size.

Satisfactory resolution (~0.6 ppm) has been achieved even with relatively high proton density (30%) with ^{13}C decoupling, moderate Larmor frequencies (500 MHz) and standard sample spinning rates (~20 kHz). In this study, a factor of 2–3 gain in sensitivity has been demonstrated for indirect detection via protons that are attached to carbon atoms. Even better enhancement has been observed for amine and amide protons due to a more favorable starting polarization in the proton-detected experiments.

Absolute SNR increases further with protonation level above 30% (~2 $^{1}H/100$ Å^3) but full protonation results in inferior SNR. The optimal combination of resolution and sensitivity is observed to be in the range of 30–50% protonation; to favor resolution and to translate these results to samples containing fewer methyl groups, the lower end of this range will likely be most generally applicable. This strategy is likely to be useful for studies of host–guest chemistry if the guest molecules can be deuterated, or in cases where synthesizing deuterated material (e.g., by catalytically exchanging protons) is less expensive than ^{13}C,^{15}N-labeled material. Whether the results are applicable to larger peptides or proteins are still an open question. Applicability to randomly factional deuteration is also yet to be explored due to higher ratio of CH and CH_2.

We have focused here on two samples containing methyl groups. The strategy of methyl-specific protonation has been established by previous solution NMR studies [54,55]. Polarization transfer from ^{1}H to ^{13}C is effective even for distances of about 5 Å, as evident in NAV correlations observed (Fig. 7 and Table 3) the methyl and amide protons couple to all ^{13}C nuclei. This demonstrates the feasibility of using methyl protons as both polarization source and readout spins even for backbone ^{13}C signals. In perdeuterated proteins which are then back-exchanged with protons, the total proton density is usually well below 1.0 $^{1}H/100$ Å^3, which is calculated for a highly compact protein GB1 with complete exchange [56], or 0.66 $^{1}H/100$ Å^3 for α-spectrin SH3 domain [57]. For membrane proteins the exchange efficiency is expected to be much lower. In comparison, protonating all methyls (but not exchangeable protons) in GB1, for example, would result in 0.81 $^{1}H/100$ Å^3. This number will typically be higher for membrane proteins, which contain a higher percentage of methyl-bearing residues.

The dilute spin reservoir will open up many new possibilities for pulse sequence design. Hohwy [58] has described a general approach to multiple-pulse homonuclear decoupling that works well in the regime of moderate-to-fast MAS. This formalism is based on the symmetry principles of Levitt et al. [59]. Both approaches require analysis of higher order AHT terms, whose convergence requires the cycle time to be much less than the inverse of the proton line width (~200 μs under ~20 kHz MAS for fully protonated sample). In our spin diluted samples with ~0.5 $^{1}H/100$ Å^3, we observe a homogeneous decay time of ~5 ms, or 100 rotor periods at 20 kHz MAS. This fact permits the use of MAS as a first-order averaging process, and multiple pulse trains as the second-order process, inverting the symmetry traditionally imposed upon this problem.

We expect that the results shown here will be advantageously combined with new probe designs that emphasize ^{1}H channel performance (e.g., sensitivity and rf efficiency and B_1 homogeneity, even in the limit of high sample salt concentration) [60]. The combination of higher magnetic fields, high speed MAS, improved probe designs, and spin dilution will yield substantial gains in sensitivity and resolution for protein solid-state NMR.

Acknowledgments

This research was supported by the University of Illinois (startup funds to C.M.R.), the Research Corporation (Research Innovation Award), the American Chemical Society (Petroleum Research Fund) and the National Science Foundation (CAREER Award, MCB 0347824). The authors thank Dr. Paul Molitor (VOICE NMR Facility, School of Chemical Sciences, University of Illinois) for technical assistance.

References

[1] A.E. McDermott, Structural and dynamic studies of proteins by solid-state NMR spectroscopy: rapid movement forward, Curr. Opin. Struct. Biol. 14 (2004) 554–561.

[2] A. McDermott, T. Polenova, A. Bockmann, K.W. Zilm, E.K. Paulsen, R.W. Martin, G.T. Montelione, Partial NMR assignments for uniformly (^{13}C,^{15}N)-enriched BPTI in the solid state, J. Biomol. NMR 16 (2000) 209–219.

[3] T.I. Igumenova, A.E. McDermott, K.W. Zilm, R.W. Martin, E.K. Paulson, A.J. Wand, Assignments of carbon NMR resonances for microcrystalline ubiquitin, J. Am. Chem. Soc. 126 (2004) 6720–6727.

[4] T.I. Igumenova, A.J. Wand, A.E. McDermott, Assignment of the backbone resonances for microcrystalline ubiquitin, J. Am. Chem. Soc. 126 (2004) 5323–5331.

[5] J. Pauli, M. Baldus, B. van Rossum, H. de Groot, H. Oschkinat, Backbone and side-chain ^{13}C and ^{15}N resonance assignments of the alpha-spectrin SH3 domain by magic angle spinning solid-state NMR at 17.6 Tesla, ChemBioChem 2 (2001) 272–281.

[6] A. Bockmann, A. Lange, A. Galinier, S. Luca, N. Giraud, M. Juy, H. Heise, R. Montserret, F. Penin, M. Baldus, Solid state NMR sequential resonance assignments and conformational analysis of the 2× 10.4 kDa dimeric form of the *Bacillus subtilis* protein Crh, J. Biomol. NMR 27 (2003) 323–339.

[7] D. Marulanda, M.L. Tasayco, A. McDermott, M. Cataldi, V. Arriaran, T. Polenova, Magic angle spinning solid-state NMR spectroscopy for structural studies of protein interfaces. Resonance assignments of differentially enriched Escherichia coli thioredoxin reassembled by fragment complementation, J. Am. Chem. Soc. 126 (2004) 16608–16620.

[8] T. Fujiwara, Y. Todokoro, H. Yanagishita, M. Tawarayama, T. Kohno, K. Wakamatsu, H. Akutsu, Signal assignments and chemical-shift structural analysis of uniformly ^{13}C,^{15}N-labeled peptide, mastoparan-X, by multidimensional solid-state NMR under magic-angle spinning, J. Biomol. NMR 28 (2004) 311–325.

[9] W.T. Franks, D.H. Zhou, B.J. Wylie, B.G. Money, D.T. Graesser, H.L. Frericks, G. Sahota, C.M. Rienstra, Magic-angle spinning solid-state NMR spectroscopy of the β1 immunoglobulin binding domain of protein G (GB1): ^{15}N and ^{13}C chemical shift assignments and conformational analysis, J. Am. Chem. Soc. 127 (2005) 12291–12305.

[10] C.M. Rienstra, L. Tucker-Kellogg, C.P. Jaroniec, M. Hohwy, B. Reif, M.T. McMahon, B. Tidor, T. Lozano-Perez, R.G. Griffin, De novo determination of peptide structure with solid-state magic-angle spinning NMR spectroscopy, Proc. Natl. Acad. Sci. USA 99 (2002) 10260–10265.

[11] K. Nomura, K. Takegoshi, T. Terao, K. Uchida, M. Kainosho, Determination of the complete structure of a uniformly labeled molecule by rotational resonance solid-state NMR in the tilted rotating frame, J. Am. Chem. Soc. 121 (1999) 4064–4065.

[12] K. Nomura, K. Takegoshi, T. Terao, K. Uchida, M. Kainosho, Three-dimensional structure determination of a uniformly labeled molecule by frequency-selective dipolar recoupling under magic-angle spinning, J. Biomol. NMR 17 (2000) 111–123.

[13] F. Castellani, B.V. Rossum, A. Diehl, M. Schubert, K. Rehbein, H. Oschkinat, Structure of a protein determined by solid-state magic-angle-spinning NMR spectroscopy, Nature 420 (2002) 98–102.

[14] A. Lange, S. Becker, K. Seidel, O. Pongs, M. Baldus, A concept for rapid protein-structure determination by solid-state NMR spectroscopy, Angew. Chem. Int. Ed. 44 (2005) 2089–2092.

[15] S. Luca, J.F. White, A.K. Sohal, D.V. Filippov, J.H. van Boom, R. Grisshammer, M. Baldus, The conformation of neurotensin bound to its G protein-coupled receptor, Proc. Natl. Acad. Sci. USA 100 (2003) 10706–10711.

[16] J. Cavanagh, W.J. Fairbrother, A.G. Palmer, N.J. Skelton, Protein NMR Spectroscopy: Principles and Practice, Academic Press, San Diego, 1996.

[17] Y. Ishii, J.P. Yesinowski, R. Tycko, Sensitivity enhancement in solid-state ^{13}C NMR of synthetic polymers and biopolymers by ^{1}H NMR detection with high-speed magic angle spinning, J. Am. Chem. Soc. 123 (2001) 2921–2922.

[18] J.S. Waugh, L.M. Huber, U. Haeberlen, Approach to high-resolution NMR in solids, Phys. Rev. Lett. 20 (1967) 180–182.

[19] M.H. Levitt, A.C. Kolbert, A. Bielecki, D.J. Ruben, High-resolution ^{1}H NMR in solids with frequency-switched multiple-pulse sequences, Solid State NMR 2 (1993) 151–163.

[20] J.D. Gross, P.R. Costa, R.G. Griffin, Tilted *n*-fold symmetric radio frequency pulse sequences: applications to CSA and heteronuclear dipolar recoupling in homonuclear dipolar coupled spin networks, J. Chem. Phys. 108 (1998) 7286–7293.

[21] B. Elena, G. de Paëpe, L. Emsley, Direct spectral optimisation of proton–proton homonuclear dipolar decoupling in solid-state NMR, Chem. Phys. Lett. 398 (2004) 532–538.

[22] M. Hohwy, P.V. Bower, H.J. Jakobsen, N.C. Nielsen, A high-order and broadband CRAMPS experiment using *z*-rotational decoupling, Chem. Phys. Lett. 273 (1997) 297–303.

[23] M. Hong, S. Yamaguchi, Sensitivity-enhanced static ^{15}N NMR of solids by 1H indirect detection, J. Magn. Reson. 150 (2001) 43–48.

[24] Y. Ishii, R. Tycko, Sensitivity enhancement in solid state 15N NMR by indirect detection with high-speed magic angle spinning, J. Magn. Reson. 142 (2000) 199–204.

[25] S. Samoson, T. Tuherm, Z. Gan, High-field high-speed MAS resolution enhancement in ^{1}H NMR spectroscopy of solids, Solid State NMR 20 (2001) 130–136.

[26] M. Ernst, A. Samoson, B.H. Meier, Low-power XiX decoupling in MAS NMR experiments, J. Magn. Reson. 163 (2003) 332–339.

[27] M. Ernst, M.A. Meier, T. Tuherm, A. Samoson, B.H. Meier, Low-power high-resolution solid-state NMR of peptides and proteins, J. Am. Chem. Soc. 126 (2004) 4764–4765.

[28] A.E. McDermott, F.J. Creuzet, A.C. Kolbert, R.G. Griffin, High-resolution magic-angle-spinning Nmr-spectra of protons in deuterated solids, J. Magn. Reson. 98 (1992) 408–413.

[29] B. Reif, R.G. Griffin, ^{1}H detected ^{1}H,^{15}N correlation spectroscopy in rotating solids, J. Magn. Reson. 160 (2003) 78–83.

[30] V. Chevelkov, B.J.v. Rossum, F. Castellani, K. Rehbein, A. Diehl, M. Hohwy, S. Steuernagel, F. Engelke, H. Oschkinat, B. Reif, ^{1}H detection in MAS solid-state NMR spectroscopy of biomacromolecules employing pulsed field gradients for residual solvent suppression, J. Am. Chem. Soc. 125 (2003) 7788–7789.

[31] E.K. Paulson, C.R. Morcombe, V. Gaponenko, B. Dancheck, R.A. Byrd, K.W. Zilm, High-sensitivity observation of dipolar exchange and NOEs between exchangeable protons in proteins by 3D solid-state NMR spectroscopy, J. Am. Chem. Soc. 125 (2003) 14222–14223.

[32] E.K. Paulson, C.R. Morcombe, V. Gaponenko, B. Dancheck, R.A. Byrd, K.W. Zilm, Sensitive high resolution inverse detection NMR spectroscopy of proteins in the solid state, J. Am. Chem. Soc. 125 (2003) 15831–15836.

[33] B. Reif, C.P. Jaroniec, C.M. Rienstra, M. Hohwy, R.G. Griffin, ^{1}H–^{1}H MAS correlation spectroscopy and distance measurements in a deuterated peptide, J. Magn. Reson. 151 (2001) 320–327.

[34] K.H. Gardner, L.E. Kay, The use of ^{2}H,^{13}C,^{15}N multidimensional NMR to study the structure and dynamics of proteins, Annu. Rev. Biophys. Biomol. Struct. 27 (1998) 357–406.

[35] J. Fiaux, E.B. Bertelsen, A.L. Horwich, K. Wuthrich, Uniform and residue-specific ^{15}N-labeling of proteins on a highly deuterated background, J. Biomol. NMR 29 (2004) 289–297.

[36] O. Halskau, N.A. Froystein, A. Muga, A. Martinez, The membrane-bound conformation of alpha-lactalbumin studied by NMR-monitored ^{1}H Exchange, J. Mol. Biol. 321 (2002) 99–110.

[37] T.J.T. Pinheiro, H. Cheng, S.H. Seeholzer, H. Roder, Direct evidence for the cooperative unfolding of cytochrome *c* in lipid membranes from ^{1}H–^{2}H exchange kinetics, J. Mol. Biol. 303 (2000) 617–626.

[38] B.A. Schulman, C. Redfield, Z.-y. Peng, C.M. Dobson, P.S. Kim, Different subdomains are most protected from hydrogen exchange in

the molten globule and native states of human [alpha]-lactalbumin, J. Mol. Biol. 253 (1995) 651–657.
[39] T.N. Earnest, J. Herzfeld, K.J. Rothschild, Polarized Fourier transform infrared spectroscopy of bacteriorhodopsin. Transmembrane alpha helices are resistant to hydrogen/deuterium exchange, Biophys. J. 58 (1990) 1539–1546.
[40] J.E. Baenziger, N. Méthot, Fourier transform infrared and hydrogen/deuterium exchange reveal an exchange-resistant core of alpha-helical peptide hydrogens in the nicotinic acetylcholine receptor, J. Biol. Chem. 270 (1995) 29129–29137.
[41] J. Sturgis, B. Robert, E. Goormaghtigh, Transmembrane helix stability: the effect of helix–helix interactions studied by Fourier transform infrared spectroscopy, Biophys. J. 74 (1998) 988–994.
[42] M.S. Vinchurkar, K.H.C. Chen, S.S.F. Yu, S.J. Kuo, H.C. Chiu, S.H. Chien, S.I. Chan, Polarized ATR-FTIR spectroscopy of the membrane-embedded domains of the particulate methane monooxygenase, Biochemistry 43 (2004) 13283–13292.
[43] L. Zheng, K.W. Fishbein, R.G. Griffin, J. Herzfeld, 2-Dimensional solid-state H-1-NMR and proton-exchange, J. Am. Chem. Soc. 115 (1993) 6254–6261.
[44] S. Hafner, H.W. Spiess, Advanced solid-state NMR spectroscopy of strongly dipolar coupled spins under fast magic angle spinning, Conc. Magn. Reson. A 10 (1998) 99–128.
[45] C. Filip, S. Hafner, I. Schnell, D.E. Demco, H.W. Spiess, Solid-state nuclear magnetic resonance spectra of dipolar-coupled multi-spin systems under fast magic angle spinning, J. Chem. Phys. 110 (1999) 423–440.
[46] E. Brunner, D. Freude, B.C. Gerstein, H. Pfeifer, Residual linewidths of NMR spectra of systems under magic-angle spinning, J. Magn. Reson. 90 (1990) 90–99.
[47] S. Ray, E. Vinogradov, G.-J. Boender, S. Vega, Proton MAS NMR spectra at high magnetic fields and high spinning frequencies: spectral simulations using Floquet theory, J. Magn. Reson. 135 (1998) 418–426.
[48] J.G. Hexem, M.H. Frey, S.J. Opella, Molecular and structural information from ^{14}N–^{13}C dipolar couplings manifested in high resolution ^{13}C NMR spectra of solids, J. Chem. Phys. 77 (1982) 3847–3856.
[49] D. Massiot, F. Fayon, M. Capron, I. King, S.L. Calvé, B. Alonso, J.-O. Durand, B. Bujoli, Z. Gan, G. Hoatson, Modelling one- and two-dimensional solid state NMR spectra, Magn. Reson. Chem. 40 (2002) 70–76.
[50] H.J. Simpson, R.E. Marsh, The crystal structure of L-alanine, Acta Cryst. 20 (1966) 550–555.
[51] C.R. Morcombe, V. Gaponenko, R.A. Byrd, K.W. Zilm, ^{13}C CPMAS spectroscopy of deuterated proteins: CP dynamics, lineshapes, and T1 relaxation, J. Am. Chem. Soc. 127 (2005) 397–404.
[52] E.K. Paulson, R.W. Martin, K.W. Zilm, Cross polarization, radio frequency field homogeneity, and circuit balancing in high field solid state NMR probes, J. Magn. Reson. 171 (2004) 314–323.
[53] A.E. Bennett, C.M. Rienstra, M. Auger, K.V. Lakshmi, R.G. Griffin, Heteronuclear decoupling in rotating solids, J. Chem. Phys. 103 (1995) 6951–6958.
[54] M.K. Rosen, K.H. Gardner, R.C. Willis, W.E. Parris, T. Pawson, L.E. Kay, Selective methyl group protonation of perdeuterated proteins, J. Mol. Biol. 263 (1996) 627–636.
[55] N.K. Goto, K.H. Gardner, G.A. Mueller, R.C. Willis, L.E. Kay, A robust and cost-effective method for the production of Val, Leu, Ile (1H-d1) methyl-protonated ^{15}N-, ^{13}C-, ^{2}H-labeled proteins, J. Biomol. NMR 13 (1999) 369–374.
[56] T. Gallagher, P. Alexander, P. Bryan, G.L. Gilliland, Two crystal structures of the B1 immunoglobulin-binding domain of streptococcal protein G and comparison with NMR, Biochemistry 33 (1994) 4721–4729.
[57] A. Musacchio, M. Noble, R. Pauptit, R. Wierenga, M. Saraste, Crystal-structure of a Src-homology-3 (Sh3) domain, Nature 359 (1992) 851–855.
[58] M. Hohwy, Multiple pulse methods in solid-state NMR: methodology for structure determination of proteins and peptides in the solid phase, Ph.D. Thesis, Department of Chemistry, University of Aarhus, 2000.
[59] P.K. Madhu, X. Zhao, M.H. Levitt, High-resolution 1H NMR in the solid state using symmetry-based pulse sequences, Chem. Phys. Lett. 346 (2001) 142–148.
[60] J.A. Stringer, C.E. Bronnimann, C.G. Mullen, D.H. Zhou, S.A. Stellfox, Y. Li, E.H. Williams, C.M. Rienstra, Reduction of RF-induced sample heating with a scroll coil resonator structure for solid-state NMR probes, J. Magn. Reson. 173 (2005) 40–48.